

OMNIMOL: Transferring Particle Physics Knowledge to Molecular Dynamics with Point-Edge Transformers

Ibrahim Elsharkawy,^{1, 2, *} Vinicius Mikuni,^{3, †} Wahid Bhimji,^{1, ‡} and Benjamin Nachman^{4, 5, §}

¹*National Energy Research Scientific Computing Center (NERSC),
Lawrence Berkeley National Laboratory, Berkeley, CA, USA*

²*Department of Physics, University of Toronto, Toronto, ON, Canada*

³*Nagoya University, Kobayashi-Maskawa Institute, Aichi 464-8602, Japan*

⁴*Department of Particle Physics and Astrophysics, Stanford University, Stanford, CA 94305, USA*

⁵*Fundamental Physics Directorate, SLAC National Accelerator Laboratory, Menlo Park, CA 94025, USA*

We present OMNIMOL, a state-of-the-art transformer-based small molecule machine-learned interatomic potential (MLIP). OMNIMOL is built by adapting OMNILEARNED, a foundation model for particle jets found in high-energy physics (HEP) experiments such as at the Large Hadron Collider (LHC). OMNILEARNED is built with a Point-Edge-Transformer (PET) and pre-trained using a diverse set of one billion particle jets. It includes an interaction-matrix attention bias that injects pairwise sub-nuclear (HEP) or atomic (molecular-dynamics) physics directly into the transformer’s attention logits, steering the network toward physically meaningful neighborhoods without sacrificing expressivity. We demonstrate OMNIMOL using the oMol dataset and find excellent performance even with relatively few examples for fine-tuning. This study lays the foundation for building interdisciplinary connections given datasets represented as collections of point clouds.

I. INTRODUCTION

Machine learning (ML) has transformed how we represent, simulate, and analyze complex physical systems. Two domains where this transformation is particularly visible are particle physics [1, 2] and molecular chemistry [3, 4] (alongside related topics like molecular structure [5]). The former pursues the fundamental structure of matter while the latter is the basis for materials design and a number of other highly impactful applications. Although different in energy scale, both subjects are governed by quantum theories and share a common data structure: (variably-sized) sets of particles in (phase) space. This is a type of structured *point cloud*. Our hypothesis is that a foundation model built for point clouds in particle physics will be useful for ML tasks operating on point clouds in computational chemistry. By construction, a foundation model for particle physics should improve diverse ML tasks across particle physics, but it is not known if transferability extends to completely different scientific disciplines.

To test the hypothesis, we adapt the recent OMNILEARNED particle physics foundation model [6–8] to molecular dynamics (MD). OMNILEARNED is trained to classify and generate particle jets, which are a ubiquitous and central component of high energy reactions. Physically, these jets emerge from quantum processes related to the radiation from energetic quarks and gluons. Due to their prevalence and complexity, jets have been driving ML developments in particle physics [9–11]. We fine-tune

OMNILEARNED on MD simulations to create OMNIMOL. Along the way, we explore multiple approaches to fine tuning the foundation model.

Our goal is to develop a machine-learned interatomic potential (MLIP) [12–21]. MLIPs aim to approximate potential energy surfaces and their gradients (i.e. forces) at a fraction of the computational cost of traditional methods, such as density functional theory (DFT) [22]. The goal is to enable large-scale and long-horizon MD. Given atomic types and coordinates $\{\vec{r} \in \mathbb{R}^3\}$, an MLIP predicts $\mathbf{E}(\{\vec{r}_i\})$, the energy of a given configuration of atoms and $\vec{F}_i(\{\vec{r}_i\})$, the forces on each atom due to the rest. These predictions can be used to ‘rollout’ the motion of a molecule over time. Accuracy is necessary but not sufficient. MD utility depends on stability, energy conservation (enforced or approximate), and consistency across molecular compositions. OMNIMOL is trained on OMOl25 [23], a large-scale molecular dataset, which provides atom positions in \mathbb{R}^3 as inputs and $\mathbf{E}(\{\vec{r}_i\})$ and $\vec{F}_i(\{\vec{r}_i\})$ in \mathbb{R}^3 as labels.

In this paper, we develop a novel point-edge-transformer MLIP architecture derived from particle physics, containing an interaction-matrix attention bias for chemically informed attention, along with equivariant and conservation constraints. Using this architecture, we achieve state-of-the-art, transformer-based small molecule MLIPs. This is the first demonstration of cross-discipline transfer for scientific point-cloud foundation models.

While industrial foundation models for natural language and images have found widespread use, there are fewer examples of cross-domain models specifically for scientific data. A number of recent works have explored multiphysics foundation models for image representations of dynamical systems [24–28]. Within the discipline of fundamental physics, the OMNICOSMOS model [29]

* ibrahim.elsharkawy@mail.utoronto.ca

† vmikuni@hepl.phys.nagoya-u.ac.jp

‡ wbhimji@lbl.gov

§ nachman@stanford.edu

has a similar setup to OMNIMOL, transferring particle physics point cloud pre-training to cosmological point clouds.

This paper is organized as follows. Section Ref. II briefly reviews the OMNILEARNED model and training protocol. Next, Sec. III introduces OMNIMOL. Equivariance and energy conservation are discussed in Sec. IV. Model training is detailed in Sec. V. Results are presented in Sec. VI and the paper ends with conclusions and outlook in Sec. VII.

II. OMNILEARN(ED)

a. Backbone and heads. OMNILEARNED is composed of a general core called the the point-edge transformer (PET) body and a number of task-specific heads. The model couples *local* attention over k -nearest neighbors with physics-inspired pairwise features and *global* transformer blocks whose attention matrices are additively biased by the same interaction terms. Four learnable tokens summarize jet information. Two task heads share the PET body: a classifier and a generator trained with diffusion/flow-matching style objectives [30].

b. Inputs Each jet is represented as an unordered variable-sized set of its constituent particles. Each particle is specified by 1) kinematic information relative to the overall jet momentum, 2) discrete Particle Identification Numbers (PIPs) that indicate the type of particle (such as proton or neutron) and 3) additional per particle information that is not always available, such as the reconstructed origin of the particle in the detector.

c. Embeddings Each jet constituent is embedded into a token space given by:

$$\vec{x}_{\text{embed}} = \vec{x}_{\text{embed}}^{\text{kinematic}} + \vec{x}_{\text{embed}}^{\text{PID}} + \vec{x}_{\text{embed}}^{\text{time}} + \vec{x}_{\text{embed}}^{\text{add}} + \vec{x}_{\text{embed}}^{\text{local}}. \quad (1)$$

Kinematic information is embedded to $\vec{x}_{\text{embed}}^{\text{kinematic}}$ via a shared multilayer perceptron (MLP), and PID information $\vec{x}_{\text{embed}}^{\text{PID}}$ is embedded via a learned lookup table. For generation, the diffusion/flow time variable is embedded via an MLP and injected through $\vec{x}_{\text{embed}}^{\text{time}}$. Finally, $\vec{x}_{\text{embed}}^{\text{add}}$ is found by embedding the additional information via another MLP.

d. Local attention. The last component of the embedding is $\vec{x}_{\text{embed}}^{\text{local}}$ and given by a local attention block. For each particle, a local neighborhood is built out of the K-nearest neighbors (with K=10) using a Euclidean L2 notion of distance. OMNILEARNED then builds a set of pairwise features $f(x_i, x_j)$ followed by an MLP that transforms each of the K^2 features $f(x_i, x_j)$ before being fed into a small local transformer block. This local block aggregates all pairwise information of the K-nearest neighbors for each jet constituent into a local embedding vector $\vec{x}_{\text{embed}}^{\text{local}}$. A diagram illustrating this block is found in Figure 1.

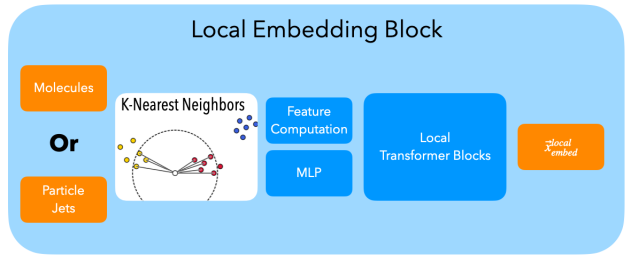


FIG. 1. Local Embedding Block, where K-Nearest Neighbors for either Molecule or Jet point-clouds are computed along with pairwise features, these are fed to an MLP, and a small local transformer resulting in $\vec{x}_{\text{embed}}^{\text{local}}$

e. Global attention and Bias After \vec{x}_{embed} is computed for each jet constituent, the unordered set of \vec{x}_{embed} is fed into large global all-to-all transformer blocks. These global self-attention components add an explicit bias to the attention logits found by computing $f(x_i, x_j)$ for all pairs of particles, and embed via an MLP into $f(x_i, x_j) \rightarrow B_{ij}$, such that the logits are set to $A_{ij}^* = A_{ij} + B_{ij}$ for $B_{ij} \in \mathbb{R}$.

f. Output Heads OMNILEARNED is built with two output heads attached to the transformer body, a classifier head, and a generator head. The generator head is composed of two smaller all-to-all transformer blocks followed by a shared MLPs applied to each token. This head is by construction *permutation equivariant*. The classifier head is composed of two "Token" Attention Blocks, which summarize jet information from the incoming body output into $n = 4$ trainable tokens. These summary tokens are then flattened and fed into an output MLP, which collapses the dimensionality to the desired number of class labels.

g. Multi-task objective. Pretraining optimizes a joint loss that combines (i) cross-entropy for supervised jet-type classification, (ii) a velocity-matching ℓ_2 loss (flow matching, equivalent to diffusion) for generation, and (iii) a classification on noised inputs term to couple the two representations. To exploit unlabeled data, the classifier head is split to predict either jet type (when labels exist) or *sample identity* (dataset classification) with equal weighting in the loss.

h. Pre-training dataset and Compute. OMNILEARNED is pretrained on over one billion jets drawn from a unified suite of open datasets. Training runs on 32–512 A100 GPUs using the Perlmutter supercomputer, employs a global batch size of 4096 for three full passes over the 1B-jet corpus using the Lion optimizer [31]. Released model sizes are small, medium, and large, with roughly 3M, 58M, 460M trainable weights.

More details regarding OMNILEARNED's architecture and training can be found in the paper Ref. [30]. A graphical depiction of OMNILEARNED's architecture can be found in Figure 2.

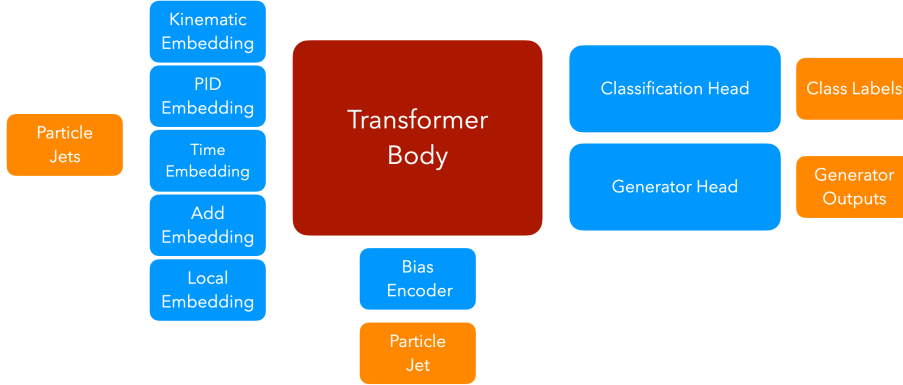


FIG. 2. OMNILEARNED’s Architecture

III. OMNIMOL

We take OMNILEARNED and swap out the input encoders and output heads to ones that match a molecular prior. These changes define OMNIMOL. As we describe OMNIMOL, the similarities between the two problems become explicit.

a. Shared Backbone and Heads. OMNIMOL uses a similar input encoders, similar heads, and the same body as OMNILEARNED. The generative head, which is by construction permutation equivariant, is repurposed for per-atom direct force prediction. A copy of this same generative head is repurposed for energy prediction, outputting a per-atom energy correction e_i that are summed over each molecule to find $\tilde{\mathbf{E}}^* = \sum_i e_i$. The quantity $\tilde{\mathbf{E}}^*$ can then be compared to the standardized molecule level label $\tilde{\mathbf{E}}$, preserving an extensive prior.

b. Inputs The model is trained on oMol, which gives molecules as an unordered variable-sized set of atoms. Each atom contains 1) positional information given by Euclidean coordinates $\vec{r} \in \mathbb{R}^3$ relative to some origin 2) discrete Atomic Numbers (Z) and 3) additional per-atom charge and spin information [23].

c. Embeddings Each atom is embedded into a token space given by:

$$\vec{x}_{\text{embed}} = \vec{x}_{\text{embed}}^{\text{pos}} + \vec{x}_{\text{embed}}^Z + \vec{x}_{\text{embed}}^{\text{add}} + \vec{x}_{\text{embed}}^{\text{local}}. \quad (2)$$

Positional information \vec{r}_i is embedded to $\vec{x}_{i,\text{embed}}^{\text{pos}}$ via a shared MLP. Atomic Number Z is embedded to \vec{x}_{embed}^Z via a learned lookup table, and $\vec{x}_{\text{embed}}^{\text{add}}$ is found by embedding additional atom charge and spin via another MLP when available.

d. Local attention The last component of the embedding is $\vec{x}_{\text{embed}}^{\text{local}}$ and given by a local attention block. For each atom, local neighborhoods defined by K-nearest neighbors (with K=15) with respect to the atoms position vector are built, and OMNIMOL then computes pairwise physical features for each pair of atoms in the

neighborhood,

$$\begin{aligned} f(\vec{r}_i, \vec{r}_j, \vec{x}_{i,\text{embed}}^{Z,\text{add}}, \vec{x}_{j,\text{embed}}^{Z,\text{add}}) = & \left[\vec{r}_i - \vec{r}_j, \|\vec{r}_i - \vec{r}_j\|, \right. \\ & \frac{1}{\|\vec{r}_i - \vec{r}_j\|}, \frac{1}{\|\vec{r}_i - \vec{r}_j\|^2}, \frac{1}{\|\vec{r}_i - \vec{r}_j\|^6}, \\ & \frac{g(\vec{x}_{i,\text{embed}}^{Z,\text{add}}, \vec{x}_{j,\text{embed}}^{Z,\text{add}})}{\|\vec{r}_i - \vec{r}_j\|}, \frac{g(\vec{x}_{i,\text{embed}}^{Z,\text{add}}, \vec{x}_{j,\text{embed}}^{Z,\text{add}})}{\|\vec{r}_i - \vec{r}_j\|^2}, \\ & \left. \frac{g(\vec{x}_{i,\text{embed}}^{Z,\text{add}}, \vec{x}_{j,\text{embed}}^{Z,\text{add}})}{\|\vec{r}_i - \vec{r}_j\|^6}, \{RBF(\vec{r}_i, \vec{r}_j)_m \mid \forall m\} \right], \end{aligned} \quad (3)$$

followed by an MLP that transforms each $f(\vec{r}_i, \vec{r}_j, \vec{x}_{i,\text{embed}}^{Z,\text{add}}, \vec{x}_{j,\text{embed}}^{Z,\text{add}})$ before being fed into a small local transformer block. The quantity $g(\vec{x}_{i,\text{embed}}^{Z,\text{add}}, \vec{x}_{j,\text{embed}}^{Z,\text{add}})$ is a learned function of atomic number embeddings and additional feature embeddings computed by an MLP. Lastly, $\{RBF(\vec{r}_i, \vec{r}_j)_k \mid \forall k\}$ is a set of radial basis functions (RBFs) used to give the MLP maximal flexibility in learning important 2-point correlations. OMNIMOL uses Gaussian RBFs given by,

$$RBF(\vec{r}_i, \vec{r}_j)_m = \exp\left(-\frac{\|\vec{r}_i - \vec{r}_j\|^2}{2\sigma_m^2}\right), \quad (4)$$

where m ranges from 0 to 30, and σ_m is evenly spaced on a range from (0.1, 10). This local block aggregates all pairwise information of the K-nearest neighbors for each atom into a local embedding vector $\vec{x}_{\text{embed}}^{\text{local}}$. A diagram illustrating this block can again be found in Figure 1.

e. Global attention and Bias After \vec{x}_{embed} is computed for each atom, the unordered set of \vec{x}_{embed} is fed into OMNILEARNED’s large all-to-all transformer blocks. These global self-attention blocks, once again, add an explicit bias to the attention logits found by computing the same chemical priors $f(\vec{r}_i, \vec{r}_j, \vec{x}_{i,\text{embed}}^{Z,\text{add}}, \vec{x}_{j,\text{embed}}^{Z,\text{add}})$ for all pairs of particles, and embed via an MLP into biases $f(\vec{r}_i, \vec{r}_j, \vec{x}_{i,\text{embed}}^{Z,\text{add}}, \vec{x}_{j,\text{embed}}^{Z,\text{add}}) \rightarrow B_{ij}$, such that the logits are again set to $A_{ij}^* = A_{ij} + B_{ij}$ for $B_{ij} \in \mathbb{R}$. An illustra-

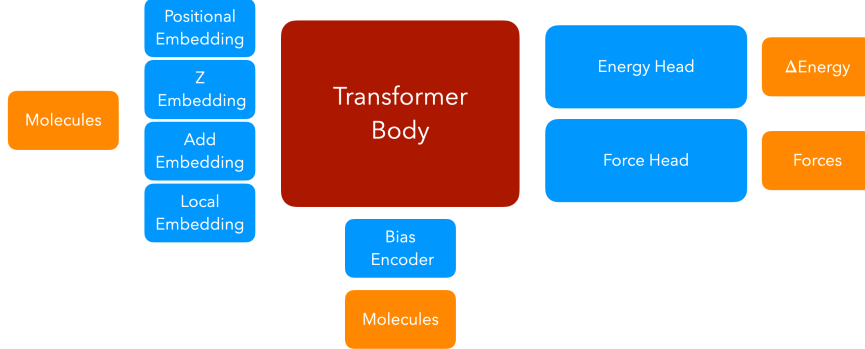


FIG. 3. OMNIMOL’s Architecture

tion of OMNIMOL’s architecture can be found in Figure 3.

IV. BUILDING IN EQUIVARIANCE AND CONSERVATION

It is often desired to encourage certain physical constraints/priors in ML models built for physical systems. For MLIPs, two constraints are desired: rotational equivariance and energy conservation.

Energy conservation implies that the forces on atom i is given by:

$$\vec{F}_i = \frac{dE(\{\vec{r}_i\})}{dr_i}. \quad (5)$$

Energy conservation is implemented in OMNIMOL by dropping the direct force head and compute forces via Eq. 5 with backpropagation. Due to the required double backpropagation, energy conservation slows down training and increases the required computation significantly. We thus only train OMNIMOL small this way, *leaving larger models to future work*.

The second constraint a MLIP is expected to satisfy is rotational equivariance. Physically, any rotation (or change of coordinates) should have no effect on the magnitude of the force on each atom, nor on the magnitude of the scalar energy for the configuration. That is, if a structure’s coordinates transform as,

$$\vec{x} \rightarrow Q\vec{x}, \quad (6)$$

for some rotation matrix Q , forces and energies should transform via,

$$E(\{\vec{r}_i\}) \rightarrow E(\{\vec{r}_i\}), \quad \vec{F}_i(\{\vec{r}_i\}) \rightarrow Q\vec{F}_i(\{\vec{r}_i\}). \quad (7)$$

OMNIMOL as described is not equivariant, due first to the many locations where raw coordinates or coordinate differences are fed to MLPs, which are not constrained to satisfy Eq. 6, and secondly due to the *direct* force head

not constrained to transform forces according to Eq. 7. To remedy this, we first use conservative OMNIMOL, we then drop the input encoder, and drop the $\vec{r}_i - \vec{r}_j$ term in the pairwise features $f(\vec{r}_i, \vec{r}_j, \vec{x}_{i,embed}^{Z,add}, \vec{x}_{j,embed}^{Z,add})$ in the local and interaction block.

We find that the removal of $\vec{r}_i - \vec{r}_j$ reduces performance significantly, and we remedy this loss by introducing angular information. In the local block, for each atom, we take its K-nearest neighbors as before. We then take two vectors defined by

$$\vec{v}_1 = \vec{r}_i - \vec{r}_j, \quad \vec{v}_2 = \vec{r}_k - \vec{r}_m, \quad (8)$$

where r_i, r_j, r_k and r_m are atoms neighboring the center of interest. We then compute the cosine between \vec{v}_1 and \vec{v}_2 and append all $\binom{K}{2}$ such angles to the features fed to the small local transformer. This addition improves performance significantly, while retaining equivariance. The architecture of the equivariant and conserving variant of OMNIMOL can be found in Fig. 4.

V. TRAINING/FINE-TUNING ON OMOL

A. Input and Label Pre-Processing

We treat each molecule in oMoL as a variable-size point cloud of atoms with associated coordinates and atomic numbers. Let a molecule be specified by $\{\mathbf{r}_i, Z_i\}_{i=1}^N$, where $\mathbf{r}_i \in \mathbb{R}^3$ are Cartesian coordinates and Z_i are atomic numbers. To remove global translation and constrain the scale, we perform a per-molecule centering by subtract the center

$$\bar{\mathbf{r}} = \frac{1}{N} \sum_{i=1}^N \mathbf{r}_i, \quad (9)$$

from all coordinates, $\tilde{\mathbf{r}}_i = \mathbf{r}_i - \bar{\mathbf{r}}$. Energies are processed to remove a simple, additive baseline corresponding to the heat of formation (a “bag-of-atoms” reference). For

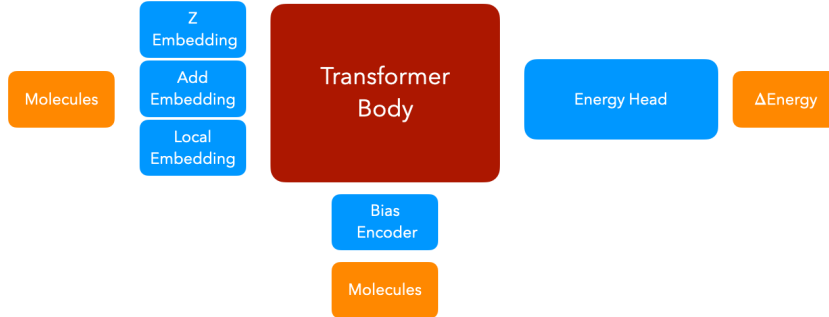


FIG. 4. Conservative and Equivariant OMNIMOL’s Architecture

each molecule, the DFT total energy E_{DFT} is decomposed as

$$E_{\text{DFT}} = \sum_i^N E_{Z_i} + \Delta E, \quad (10)$$

where E_{Z_i} is the energy of an isolated atom with a given Z_i , N is the total number of atoms in the molecule. We use ΔE as the primary target, and further apply a global standardization across the training set:

$$\tilde{E} = \frac{\Delta E - \mu_{\Delta E}}{\sigma_{\Delta E}}, \quad (11)$$

where $\mu_{\Delta E}$ and $\sigma_{\Delta E}$ are the mean and standard deviation of ΔE over training molecules. This yields dimensionless energy targets with approximately unit variance. Finally, we standardize the components of $\tilde{\mathbf{F}}_i$ across the training set to have zero mean and unit variance per Cartesian direction, yielding force targets that are numerically comparable to the standardized energies.

B. Training Objective, Optimizer and Scheduler

We train with the sum of the mean absolute error (MAE) of energies and the per component per atom MAE of forces weighted by $\lambda_E = 1$ and $\lambda_F = 10$, such that our loss function is given by:

$$\mathcal{L} = \lambda_E |\tilde{\mathbf{E}} - \tilde{\mathbf{E}}^*| + \frac{\lambda_F}{3N} \sum_i^N \sum_j^3 |\tilde{\mathbf{F}}_{ij} - \tilde{\mathbf{F}}_{ij}^*|. \quad (12)$$

For the optimizer, we find the standard ADAMW [32] to be effective with learning rate $\eta = 1e-3$ for OMNIMOL small, and $\eta = 3e-4$ for OMNIMOL medium. We keep other optimizer parameters such as $\beta_1, \beta_2 = .95, .99$ and weight decay $1e-4$ fixed for all runs.

Finally, we employ a `OneCycle` learning-rate policy for all trainings, which ramps the learning rate up and then

down over the course of training. This schedule encourages rapid exploration early on, followed by a controlled annealing phase that reduces overfitting and improves convergence [33]. We train all runs for 100 passes of the data and choose the checkpoint with the best validation loss.

We consider two fine-tuning strategies, as described in the next two subsections.

C. LoRA Fine-Tuning

We fine-tune a jet-pretrained PET backbone on oMoL using Low-Rank Adaptation (LoRA) [34] applied *only* to the transformer body. The base backbone consists of stacked transformer blocks with multi-head self-attention and feed-forward (MLP) sublayers. Each attention block involves learned projection matrices for queries, keys, values, and output (often denoted W_Q, W_K, W_V, W_O), while the MLP consists of linear layers with weights W_{MLP} .

In our setup, all *base* weights in the transformer body are frozen; we introduce LoRA adapters only on the body matrices, $W_Q, W_K, W_V, W_O, W_{\text{MLP}}$. For each such matrix $W \in \mathbb{R}^{d_{\text{out}} \times d_{\text{in}}}$, we parameterize a low-rank update

$$W' = W + \Delta W, \quad \Delta W = \frac{\alpha}{r} BA, \quad (13)$$

where $A \in \mathbb{R}^{r \times d_{\text{in}}}$ and $B \in \mathbb{R}^{d_{\text{out}} \times r}$ are trainable LoRA parameters, r is the LoRA rank, and α is a scaling factor. In our experiments we set, $r = 96$ for all adapted matrices. The original W remain fixed with gradients disabled. All LoRA runs satisfy $\#\text{trainable parameters} < \#\text{parameters}$ from scratch.

Alongside the LoRA parameters, we train:

1. the *molecular encoders* that embed molecules into $\vec{x}_{\text{embed}} = \vec{x}_{\text{embed}}^{\text{pos}} + \vec{x}_{\text{embed}}^Z + \vec{x}_{\text{embed}}^{\text{add}} + \vec{x}_{\text{embed}}^{\text{local}}$.
2. the *bias MLP* that transforms all pairwise physics priors into a transformer bias $f(\vec{r}_i, \vec{r}_j, \vec{x}_{i,\text{embed}}^Z, \vec{x}_{j,\text{embed}}^Z) \rightarrow B_{ij}$.

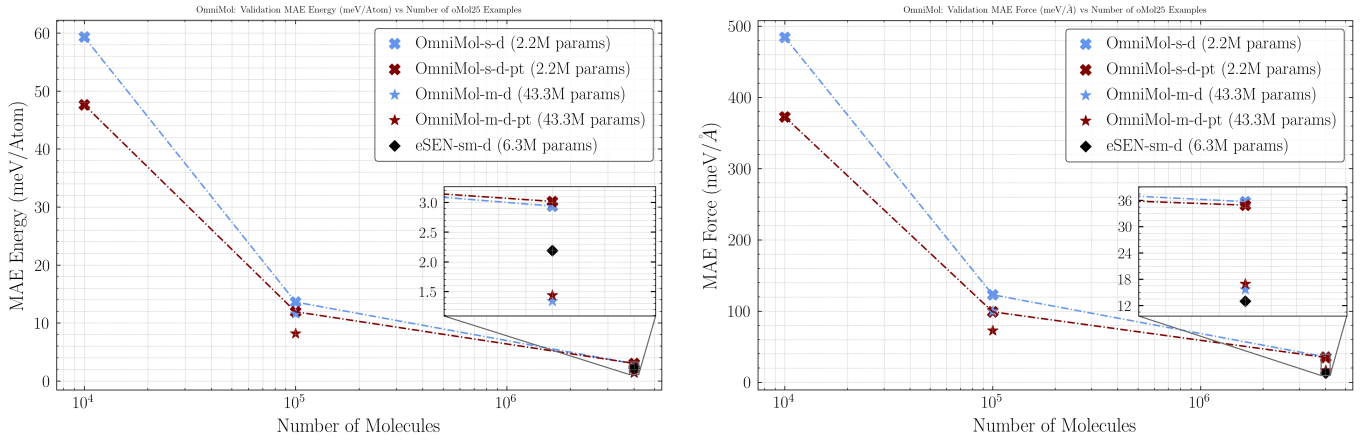


FIG. 5. Scaling behavior for (left) energy and (right) forces of OMNI-MOL direct small and medium pre-trained and from scratch. Finetuning with ten and one hundred thousand molecules on OMNI-MOL small proceeds with LoRA, 4 million and OMNI-MOL medium with full finetuning.

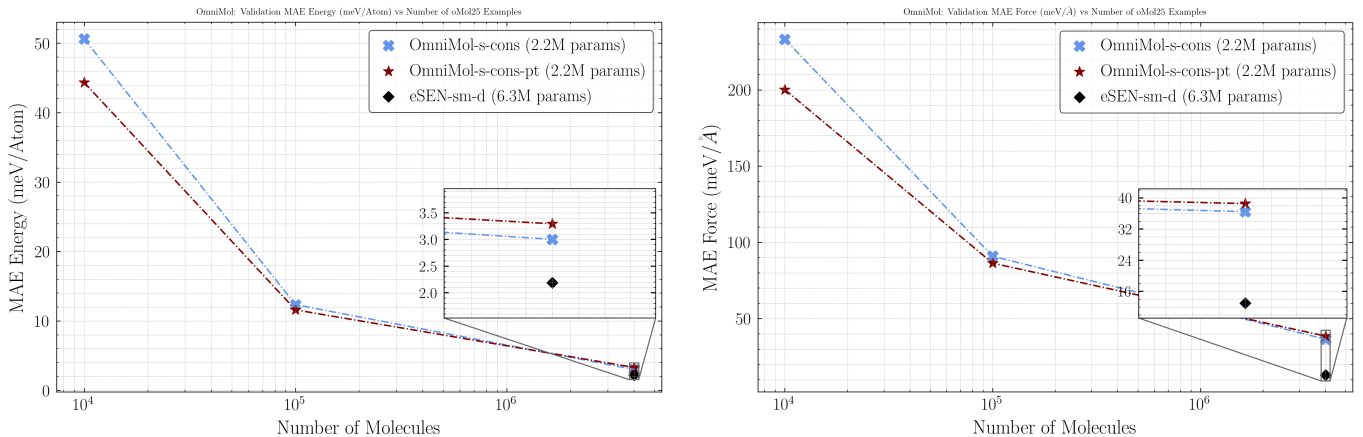


FIG. 6. Scaling behavior for (left) energy and (right) forces of conservative and equivariant OMNI-MOL small pre-trained and from scratch. Finetuning with ten and one hundred thousand molecules proceeds with LoRA, 4 million with full finetuning.

3. the *task heads* that map the transformer representation to energy and force predictions.

a. Embedding Adapters Finally, we introduce an "embedding adapting" layer. These are a per-token gated residual MLP placed in between the trained from scratch input encoders and the pre-trained transformers that modify learned embeddings \vec{x}_{embed} by:

$$\vec{x}_{\text{embed}}^* = \vec{x}_{\text{embed}} + \tanh(\alpha) * f_{\text{MLP}}(\vec{x}_{\text{embed}}). \quad (14)$$

with a learnable gating scalar α . We find this extra layer results in well-conditioned training.

D. Full Fine-Tuning

We observe LoRA to be performant for finetuning on small subsets of oMol ($>\mathcal{O}(100k)$), but we find the benefits smaller at bigger architectures. Given that LoRA is

generally best used for fast adaptation on small datasets this is expected [34–36].

To remedy this, we enable full finetuning. For full finetuning, we load *all* weights that match in dimensionality in both the body and input encoders. We do not load any weights in the energy and force heads and we do not introduce embedding adapters. With full-finetuning, we find that the first epoch validation loss is significantly lower for pretrained models, approaching a factor of two improvement for OMNI-MOL medium.

VI. EVALUATION

In this section, we compare the performance of OMNI-MOL to other MLIPs, comparing MAE of energies and forces. In Table II and Table III, we observe the strong benefit of jet-physics pre-training when training with a small number of molecules ($\sim 100k$ or less) or with a

TABLE I. Comparison between the performance reported for different algorithms trained on oMol 4M and evaluated on the Val-Comp Dataset. Bold results represent the algorithm with highest performance.

MAE $meV \downarrow$	Energy $meV/Atom$	Forces $meV/\text{\AA}$
<i>GNN Baselines</i>		
eSEN-sm-d (6.3M)	2.19	13.01
eSEN-sm-cons (6.3M)	1.89	11.10
eSEN-md-d (50.7 M)	1.32	6.78
<i>Transformer MLIPs</i>		
Transformer-1B (1B) ^a	1.99	18.35
TransIP (302M) ^b	10.79	103.8
<i>Ours</i>		
OMNIMOL-S-D (2.2M)	2.939	35.748
OMNIMOL-S-D-PT (2.2M)	3.018	34.938
OMNIMOL-S-CONS (2M)	2.939	35.748
OMNIMOL-S-CONS-PT (2M)	3.29	38.55
OMNIMOL-M-D (43.3M)	1.341	15.687
OMNIMOL-M-D-PT (43.3M)	1.441	16.980

^a Model from [37]

^b Model from [38]

few number of passes over oMol-4M (two epochs in our example). In this low-compute or low-data regime, pre-training can improve performance by up to 50%, potentially reducing the required compute for a given performance target. The pre-training advantage is reduced as more molecular training examples and more compute is provided as seen in Table I. We also observe the benefit of the equivariant + conservative model, with significantly improved performance (especially forces) when training with the small subset of molecules. We again observe this raw MAE advantage of the equivariant + conservative model disappearing with large number of molecules. This provides valuable intuition for how to understand jet pre-training: a strong inductive bias, and like other inductive bias (such as equivariance), most useful when training data is limited, i.e. the bitter lesson [39–41]. Important to highlight, OMNIMOL-M outperforms the 1-billion parameter transformer model trained in Ref. [37], with *20x fewer* parameters, and thus representing the current best transformer MLIP.

TABLE II. Comparison between the performance of OMNIMOL variants trained on a **100k subset** of oMol and evaluated on the Val-Comp Dataset. Bold results represent the algorithm with highest performance.

MAE $meV \downarrow$	Energy $meV/Atom$	Forces $meV/\text{\AA}$
OMNIMOL-S-D (2.2M)	13.598	122.918
Pre-Training Advantage (%)	+12.3%	+19.5%
OMNIMOL-S-D-PT (2.2M)	11.924	98.995
OMNIMOL-S-CONS (2M)	12.338	90.925
Pre-Training Advantage (%)	+6.1%	+5.0%
OMNIMOL-S-CONS-PT (2M)	11.586	86.363
OMNIMOL-M-D (43.3M)	11.582	99.758
Pre-Training Advantage (%)	+29.4%	+26.9%
OMNIMOL-M-D-PT (43.3M)	8.175	72.876

TABLE III. Comparison between the performance of OMNIMOL variants trained with **only two passes** of oMol 4M and evaluated on the Val-Comp Dataset. Bold results represent the algorithm with highest performance.

MAE $meV \downarrow$	Energy $meV/Atom$	Forces $meV/\text{\AA}$
OMNIMOL-S-D (2.2M)	73.767	395.76
Pre-Training Advantage (%)	+34.7%	+29.4%
OMNIMOL-S-D-PT (2.2M)	48.174	279.29
OMNIMOL-S-CONS (2M)	84.62	252.77
Pre-Training Advantage (%)	-20.1%	+17.6%
OMNIMOL-S-CONS-PT (2M)	101.59	208.34
OMNIMOL-M-D (43.3M)	62.34	298.63
Pre-Training Advantage (%)	+54.6%	+56.9%
OMNIMOL-M-D-PT (43.3M)	28.31	128.57

A. Transformer Benefits: Scaling and Compute

We would like to highlight the scaling of OMNIMOL. Transformers are known to be data and parameter-hungry and often under perform relative to other architectures if either is insufficient [42, 43]. On the other hand, they seem to be superior in scaling, outperforming architectures with better priors with sufficient data and size [37, 44–46]. This pattern appears to extend to MLIPs as well. Recent work shows that transformers for molecular energies and forces follow clean power-law scaling with model size and show no signs of saturation up to 1B parameters, and thus their scaling fits can successfully extrapolate to larger models [37]. Importantly, the same study also finds that these transformers can train and run faster (in wall-clock time) than sparse message-passing GNNs despite large parameter counts, benefiting from the plethora of hardware optimizations built for transformers [37]. We thus expect OMNIMOL to scale well, and hints of this can be seen in Figure 7, where we compare the model size scaling of OMNIMOL and the non-transformer graph network eSEN.

VII. CONCLUSION AND OUTLOOK

We present OMNIMOL, a cross-domain machine-learned interatomic potential obtained by adapting a particle physics jet-pretrained Point-Edge Transformer (PET) backbone to molecular energies and forces. We studied both parameter-efficient adaptation (LoRA in the transformer body) and full fine-tuning from jet physics pre-training, showing that cross-domain initialization can substantially accelerate early optimization and improve accuracy in the low-data regime. Looking ahead, we leave several important directions to future work. First, we plan to scale OMNIMOL with a larger backbones and more molecular training data, to fully probe the regime where transformer scaling dominates. Extending energy-conserving and equivariant training to *large* models for example is a particularly high-impact target. Finally, we will broaden evaluation beyond static

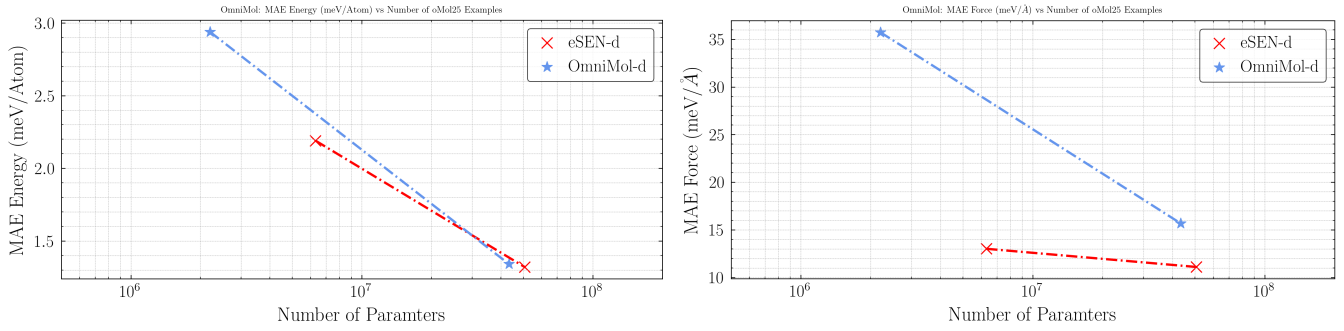


FIG. 7. Scaling behavior for energy and forces with respect to model size for OMNI-MOL-d from scratch and eSEN-d

energy and force error to better characterize where cross-domain transfer most reliably improves scientific utility.

Even though we focus on MLIPs, the lessons learned here could have widespread utility. Many scientific domains describe the systems of interest as unordered sets of interacting bodies, each endowed with attributes. Point clouds are widespread in science and it would be interesting to explore further connections in the future.

CODE AVAILABILITY

The code for this paper can be found at <https://github.com/ibrahimEls/OmniMol>.

ACKNOWLEDGMENTS

We thank Samuel Blau, Ray Gao, Brandon Wood, Daniel Levine, and Abdulrahman Aldoosary for interest-

ing discussions which significantly deepened our knowledge of the needs of the field. In addition, we thank Joschka Birk for many lessons in model development. VM is supported by JST EXPERT-J, Japan Grant Number JPMJEX2509. BN is supported by the U.S. Department of Energy (DOE), Office of Science under contract DE-AC02-76SF00515. This research used resources of the National Energy Research Scientific Computing Center, a DOE Office of Science User Facility supported by the Office of Science of the U.S. Department of Energy under Contract No. DE-AC02-05CH11231 using NERSC awards ERCAP0034229, HEP-ERCAP0021099 and HEP-ERCAP0028249.

-
- [1] A. Radovic, M. Williams, D. Rousseau, M. Kagan, D. Bonacorsi, A. Himmel, A. Aurisano, K. Terao, and T. Wongjirad, *Nature* **560**, 41 (2018).
- [2] G. Karagiorgi, G. Kasieczka, S. Kravitz, B. Nachman, and D. Shih, *Nature Reviews Physics* **4**, 399 (2022).
- [3] O. A. von Lilienfeld, K.-R. Müller, and A. Tkatchenko, *Nature Reviews Chemistry* **4**, 347 (2020).
- [4] J. Behler, *Chemical Reviews* **121**, 10037 (2021).
- [5] J. Jumper, R. Evans, A. Pritzel, T. Green, M. Figurnov, O. Ronneberger, K. Tunyasuvunakool, R. Bates, A. Žídek, A. Potapenko, A. Bridgland, C. Meyer, S. A. A. Kohl, A. J. Ballard, A. Cowie, B. Romera-Paredes, S. Nikolov, R. Jain, J. Adler, T. Back, S. Petersen, D. Reiman, E. Clancy, M. Zielinski, M. Steinegger, M. Pacholska, T. Berghammer, S. Bodenstein, D. Silver, O. Vinyals, A. W. Senior, K. Kavukcuoglu, P. Kohli, and D. Hassabis, *Nature* **596**, 583 (2021).
- [6] V. Mikuni and B. Nachman, *Phys. Rev. D* **111**, L051504 (2025), [arXiv:2404.16091 \[hep-ph\]](https://arxiv.org/abs/2404.16091).
- [7] V. Mikuni and B. Nachman, *Phys. Rev. D* **111**, 054015 (2025), [arXiv:2502.14652 \[hep-ph\]](https://arxiv.org/abs/2502.14652).
- [8] W. Bhimji, C. Harris, V. Mikuni, and B. Nachman, (2025), [arXiv:2510.24066 \[hep-ph\]](https://arxiv.org/abs/2510.24066).
- [9] A. J. Larkoski, I. Moult, and B. Nachman, *Phys. Rept.* **841**, 1 (2020), [arXiv:1709.04464 \[hep-ph\]](https://arxiv.org/abs/1709.04464).
- [10] A. Butter *et al.*, *SciPost Phys.* **7**, 014 (2019), [arXiv:1902.09914 \[hep-ph\]](https://arxiv.org/abs/1902.09914).
- [11] M. Feickert and B. Nachman, (2021), [arXiv:2102.02770 \[hep-ph\]](https://arxiv.org/abs/2102.02770).
- [12] J. S. Smith, O. Isayev, and A. E. Roitberg, *Chemical Science* **8**, 3192 (2017).
- [13] K. Yao, J. E. Herr, D. Toth, R. McIntyre, and J. Parkhill, *Chemical Science* **9**, 2261 (2018).
- [14] J. Behler and M. Parrinello, *Physical Review Letters* **98**, 146401 (2007).
- [15] K. T. Schütt, P.-J. Kindermans, H. E. Sauceda, S. Chmiela, A. Tkatchenko, and K.-R. Müller, in *Advances in Neural Information Processing Systems*, Vol. 30 (2017).
- [16] J. Gasteiger, F. Becker, and S. Günnemann, in *Advances in Neural Information Processing Systems*, Vol. 34 (2021) pp. 6790–6802.

- [17] S. Batzner, A. Musaelian, L. Sun, M. Geiger, J. P. Mailoa, M. Kornbluth, N. Molinari, T. E. Smidt, and B. Kozinsky, *Nature Communications* **13**, 2453 (2022).
- [18] I. Batatia, D. P. Kovács, G. N. C. Simm, C. Ortner, and G. Csányi, in *Advances in Neural Information Processing Systems* (2022).
- [19] Y.-L. Liao, B. Wood, A. Das, and T. Smidt, arXiv preprint arXiv:2306.12059 (2024).
- [20] E. Qu and A. S. Krishnapriyan, in *Advances in Neural Information Processing Systems* (2024) pp. 139030–139053.
- [21] X. Fu, B. M. Wood, L. Barroso-Luque, D. S. Levine, M. Gao, M. Dzamba, and C. L. Zitnick, arXiv preprint arXiv:2502.12147 (2025).
- [22] N. Mardirossian and M. Head-Gordon, *Molecular Physics* **115**, 2315 (2017).
- [23] D. S. Levine, M. Shuaibi, E. W. C. Spotte-Smith, M. G. Taylor, M. R. Hasyim, K. Michel, I. Batatia, G. Csányi, M. Dzamba, P. Eastman, N. C. Frey, X. Fu, V. Gharakhanyan, A. S. Krishnapriyan, J. A. Rackers, S. Raja, A. Rizvi, A. S. Rosen, Z. Ulissi, S. Vargas, C. L. Zitnick, S. M. Blau, and B. M. Wood, “The open molecules 2025 (omol25) dataset, evaluations, and models,” (2025), arXiv:2505.08762 [physics.chem-ph].
- [24] M. McCabe, P. Mukhopadhyay, T. Marwah, B. R.-S. Blancard, F. Rozet, C. Diaconu, L. Meyer, K. W. K. Wong, H. Sotoudeh, A. Bietti, I. Espejo, R. Fear, S. Golkar, T. Hehir, K. Hirashima, G. Krawezik, F. Lanusse, R. Morel, R. Ohana, L. Parker, M. Pettee, J. Shen, K. Cho, M. Cranmer, and S. Ho, “Walrus: A cross-domain foundation model for continuum dynamics,” (2025), arXiv:2511.15684 [cs.LG].
- [25] M. Herde, B. Raonić, T. Rohner, R. Käppeli, R. Molinaro, E. de Bézenac, and S. Mishra, in *Advances in Neural Information Processing Systems*, Vol. 37 (2024) arXiv:2405.19101 [cs.LG].
- [26] M. McCabe, B. R.-S. Blancard, L. H. Parker, R. Ohana, M. Cranmer, A. Bietti, M. Eickenberg, S. Golkar, G. Krawezik, F. Lanusse, M. Pettee, T. Tesileanu, K. Cho, and S. Ho, in *Advances in Neural Information Processing Systems*, Vol. 37 (2024).
- [27] Y. Liu, J. Sun, X. He, G. Pinney, Z. Zhang, and H. Schaeffer, arXiv preprint arXiv:2409.09811 (2024).
- [28] F. Wiesner, M. Wessling, and S. Baek, “Towards a physics foundation model,” (2025), arXiv:2509.13805 [cs.LG].
- [29] V. Mikuni, I. Elsharkawy, and B. Nachman, “Omnocosmos: Transferring particle physics knowledge across the cosmos,” (2025), arXiv:2512.24422 [astro-ph.CO].
- [30] W. Bhimji, C. Harris, V. Mikuni, and B. Nachman, (2025), 10.48550/arXiv.2510.24066, arXiv:2510.24066 [hep-ph].
- [31] X. Chen, C. Liang, D. Huang, E. Real, K. Wang, Y. Liu, H. Pham, X. Dong, T. Luong, C.-J. Hsieh, Y. Lu, and Q. V. Le, “Symbolic discovery of optimization algorithms,” (2023), arXiv:2302.06675 [cs.LG].
- [32] I. Loshchilov and F. Hutter, “Decoupled weight decay regularization,” (2019), arXiv:1711.05101 [cs.LG].
- [33] L. N. Smith and N. Topin, “Super-convergence: Very fast training of neural networks using large learning rates,” (2018), arXiv:1708.07120 [cs.LG].
- [34] E. J. Hu, Y. Shen, P. Wallis, Z. Allen-Zhu, Y. Li, S. Wang, L. Wang, and W. Chen, “Lora: Low-rank adaptation of large language models,” (2021), arXiv:2106.09685 [cs.CL].
- [35] G. Chen, F. Liu, Z. Meng, and S. Liang, in *Proceedings of the 2022 Conference on Empirical Methods in Natural Language Processing (EMNLP)* (2022) arXiv:2202.07962 [cs.CL].
- [36] N. Ding, Y. Qin, G. Yang, F. Wei, Z. Yang, Y. Su, S. Hu, Y. Chen, *et al.*, *Nature Machine Intelligence* **5**, 220 (2023).
- [37] T. Kreiman, Y. Bai, F. Atieh, E. Weaver, E. Qu, and A. S. Krishnapriyan, “Transformers discover molecular structure without graph priors,” (2025), arXiv:2510.02259 [cs.LG].
- [38] A. A. Elhag, A. Raja, A. Morehead, S. M. Blau, G. M. Morris, and M. M. Bronstein, “Learning interatomic potentials without explicit equivariance,” (2025), arXiv:2510.00027 [cs.LG].
- [39] R. S. Sutton, “The bitter lesson,” <https://www.incompleteideas.net/IncIdeas/BitterLesson.html> (2019), published March 13, 2019. A commonly used PDF mirror is https://www.cs.utexas.edu/~eunsol/courses/data/bitter_lesson.pdf.
- [40] M. Yousefi and J. Collins, “Learning the bitter lesson: Empirical evidence from 20 years of cvpr proceedings,” (2024), also appears as EMNLP 2024 NLP4Science workshop paper (per arXiv comments), arXiv:2410.09649 [cs.CV].
- [41] M. Wu, W. Wang, S. Liu, H. Yin, X. Wang, Y. Zhao, C. Lyu, L. Wang, W. Luo, and K. Zhang, “The bitter lesson learned from 2,000+ multilingual benchmarks,” (2025), arXiv:2504.15521 [cs.CL].
- [42] A. Dosovitskiy, L. Beyer, A. Kolesnikov, D. Weissenborn, X. Zhai, T. Unterthiner, M. Dehghani, M. Minderer, G. Heigold, S. Gelly, J. Uszkoreit, and N. Houlsby, “An image is worth 16x16 words: Transformers for image recognition at scale,” (2020), arXiv:2010.11929 [cs.CV].
- [43] H. Touvron, M. Cord, M. Douze, F. Massa, A. Sablayrolles, and H. Jégou, in *Proceedings of the 38th International Conference on Machine Learning (ICML)*, Proceedings of Machine Learning Research, Vol. 139 (2021).
- [44] J. Kaplan, S. McCandlish, T. Henighan, T. B. Brown, B. Chess, R. Child, S. Gray, A. Radford, J. Wu, and D. Amodei, “Scaling laws for neural language models,” (2020), arXiv:2001.08361 [cs.LG].
- [45] J. Hoffmann, S. Borgeaud, A. Mensch, E. Buchatskaya, T. Cai, E. Rutherford, D. de Las Casas, L. A. Hendricks, J. Welbl, A. Clark, T. Hennigan, E. Noland, K. Millican, G. van den Driessche, B. Damoc, A. Guy, S. Osindero, K. Simonyan, E. Elsen, O. Vinyals, J. W. Rae, and L. Sifre, in *Advances in Neural Information Processing Systems (NeurIPS)* (2022) arXiv:2203.15556 [cs.CL].
- [46] X. Zhai, A. Kolesnikov, N. Houlsby, and L. Beyer, in *Proceedings of the IEEE/CVF Conference on Computer Vision and Pattern Recognition (CVPR)* (2022) arXiv:2106.04560 [cs.CV].